Electrochemical Doping of Halide Perovskites by Noble Metal Interstitial Cations

*Ross A. Kerner, Ayala V. Cohen, Zhaojian Xu, Ahmad R. Kirmani, So Yeon Park, Steven P. Harvey, John P. Murphy, Robert C. Cawthorn, Noel C. Giebink, Joseph M. Luther, Kai Zhu, Joseph J. Berry, Leeor Kronik, and Barry P. Rand**

Metal halide perovskites are an attractive class of semiconductors, but it has proven difficult to control their electronic doping by conventional strategies due to screening and compensation by mobile ions or ionic defects. Noble-metal interstitials represent an under-studied class of extrinsic defects that plausibly influence many perovskite-based devices. In this work, doping of metal halide perovskites is studied by electrochemically formed Au^+ interstitial ions, combining experimental data on devices with a computational analysis of Au^+ interstitial defects based on density functional theory (DFT). Analysis suggests that Au^+ cations can be easily formed and migrate through the perovskite bulk via the same sites as iodine interstitials (I_i^+). However, whereas I_i^+ compensates n-type doping by electron capture, the noble-metal interstitials act as quasi-stable n-dopants. Experimentally, voltage-dependent, dynamic doping by current density–time (J–t), electrochemical impedance, and photoluminescence measurements are characterized. These results provide deeper insight into the potential beneficial and detrimental impacts of metal electrode reactions on long-term performance of perovskite photovoltaic and light-emitting diodes, as well as offer an alternative doping explanation for the valence switching mechanism of halide-perovskite-based neuromorphic and memristive devices.

1. Introduction

Control over the electronic doping of metal halide semiconductor materials has proven a significant challenge.[1,2] Early on, motion of native ion defects in halide perovskite devices and associated compensation of ionic charge by electronic carriers[3] were inferred from observations of unique phenomena, for example, current–voltage hysteresis, giant dielectric constants,[4] and switchable photovoltaic polarity.[5,6] Despite the challenge introduced by mobile ions, many strategies have been applied in an attempt to dope perovskites including substitution of lattice ions,[7–15] chemical reactions with vapors,[16–18] treatment with molecular oxidizers and reducers,[19–24] and electrochemical techniques.[25–28] However, to the best of our knowledge, there are no direct and unambiguous demonstrations of "textbook" electronic doping modulation in halide perovskites, which would have well-defined effects on material properties such as conductivity, work function,

R. A. Kerner, A. R. Kirmani, S. Y. Park, S. P. Harvey, J. M. Luther, K. Zhu, J. J. Berry
National Renewable Energy Laboratory
Golden, CO 80401, USA

A. V. Cohen, L. Kronik
Department of Molecular Chemistry and Materials Science
Weizmann Institute of Science
Rehovoth 76100, Israel

Z. Xu, B. P. Rand
Department of Electrical Engineering
Princeton University
Princeton, NJ 08544, USA
E-mail: brand@princeton.edu

J. P. Murphy, R. C. Cawthorn, N. C. Giebink
Department of Electrical Engineering
The Pennsylvania State University
University Park, PA 16802, USA

J. J. Berry
Department of Physics
University of Colorado Boulder
Boulder, CO 80309, USA

J. J. Berry
Renewable and Sustainable Energy Institute
University of Colorado Boulder
Boulder, CO 80309, USA

B. P. Rand
Andlinger Center for Energy and the Environment
Princeton University
Princeton, NJ 08544, USA

photoluminescence (PL), and device properties.[1,2] As anticipated by early ion migration models, the difficulty arises from ionic defects in halide perovskites (labile protons, halide vacancies, interstitials, etc.); due to low thermodynamic and kinetic energy barriers, these defects are easily formed, are mobile at room temperature, and participate in reduction/oxidation (redox) reactions (e.g., iodine interstitial $I_i^+/I_i^0/I_i^-$ interconversion).[29] The mobile, reactive, and amphoteric defects appear to have a relatively small impact on optoelectronic properties like carrier recombination, but they effectively negate any attempt to substantially alter the carrier concentration or space charge regions in the bulk, resulting in nearly intrinsic behavior and pinning of the Fermi energy to a limited range.[30–32]

Recent studies establish the importance of differently charged halide interstitial species, $X_i^{+/0/-}$ (i.e., $I_i^{+/0/-}$ in iodide and mixed compositions, or $Br_i^{+/0/-}$ in pure bromide or bromide:chloride compositions).[33–36] Redox conversion between the different charge states may help explain observations such as "trap filling",[22,25,37] though it should be recognized that X_i^+ and X_i^- are distinct in that X_i^+ contains only halogen bonds while X_i^- is primarily bonded to Pb, and the trap properties are predicted to change upon conversion.[34] Interestingly, monovalent noble metal cations have been proposed to be chemically similar to I_i^+ defects, occupying the same site and possessing the same coordination to neighboring halides.[38–40] Unlike I_i^+, noble metal interstitial defects have not been widely acknowledged to contribute to ion migration phenomena and associated optoelectronic changes, perhaps due to the experimental difficulty associated with direct detection of interstitial species. In this work, we combine experimental and computational results that substantiate a compelling case for the electrochemical formation of Au_i^+ defects at solid-state (halide perovskite)/(Au electrode) interfaces having a strong influence on electronic doping, current density–time (J–t), current density–voltage (J–V), impedance, and PL characteristics.

2. Results and Discussion

2.1. MAPbI$_3$:Au$_i^+$ Computational Predictions

Figure 1a shows an optimized structure of an Au_i^+ cation residing within a Pb halide octahedral interstice of, in this case, methylammonium lead triiodide (MAPbI$_3$, with methylammonium ions omitted for clarity). The structure closely resembles that of the I_i^+ defect. Figure 1b displays the formation enthalpy of Au_i^+ and Au_i^0 as a function of electrochemical potential, μ, as computed by density functional theory (DFT). Importantly, the $Au_i^{+/0}$ thermodynamic transition level (intersection of Au^0 and Au^+ curves) is found to lie at or slightly above the conduction band minimum (CBM) of MAPbI$_3$ ($\approx$1.5–1.6 eV) suggesting the Au_i^+ oxidation state as stable in the perovskite bulk if μ remains within the bandgap (though "hot" electrons or lattice fluctuations[41] may still facilitate $Au_i^{+/0}$ reduction). Because Au_i remains positively charged, its formation enthalpy is sensitive to μ, increasing by $\approx$1.5 eV (bandgap) as the electrochemical potential shifts from the valence band maximum (VBM) to the CBM. This tends to thermodynamically inhibit Au_i^+ formation as μ increases.
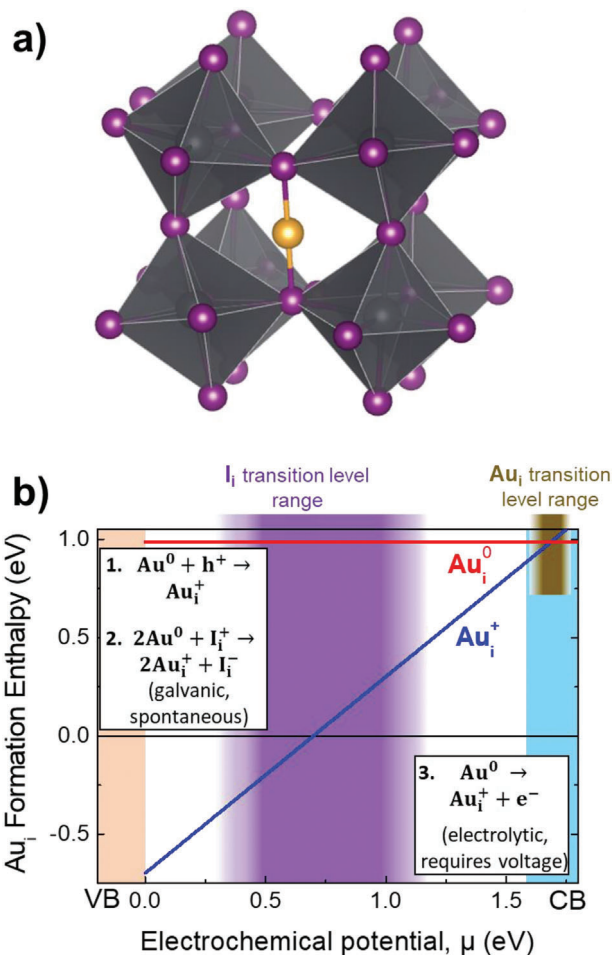
Figure 1. a) Structure of Au_i^+ (yellow atom) in MAPbI$_3$ (methylammonium omitted for clarity) computed using a $2 \times 2 \times 2$ tetragonal supercell. b) Computed formation enthalpy for a Au_i^+ defect as a function of the perovskite electrochemical potential, μ, referenced to the valence band (VB) maximum (0 eV). Also shown is the conduction band (CB) and the approximate range of the I_i transition level, as computed in the literature.[34,36]

When μ is close to the VBM (i.e., the perovskite is strongly p-type), the formation enthalpy is lowest and, based on the experimental data presented below, may even lead to galvanic (spontaneous) behavior. As μ increases and nears the CBM, the computed Au_i^+ formation enthalpy is largest and the reaction becomes more electrolytic, which is to say that an external potential must be applied to overcome a positive free energy formation. Thus, application of a positive voltage to a perovskite/Au interface should induce larger concentrations of Au_i^+ and an increase in n-type doping, via reaction 3 in Figure 1b. In this situation, n-type doping represents an out-of-equilibrium condition, such that the electrolytically induced Au_i^+ and n-type doping will return to equilibrium when the external bias is removed (unless a metastable condition is induced). We do not attempt to determine a precise value for the formation energy owing to inherent limitations of the enthalpy calculation, as well as the neglect of entropic terms.[42] However, the above qualitative analysis suffices to predict the general behavior, identify measurable quantities, and properly design experiments.
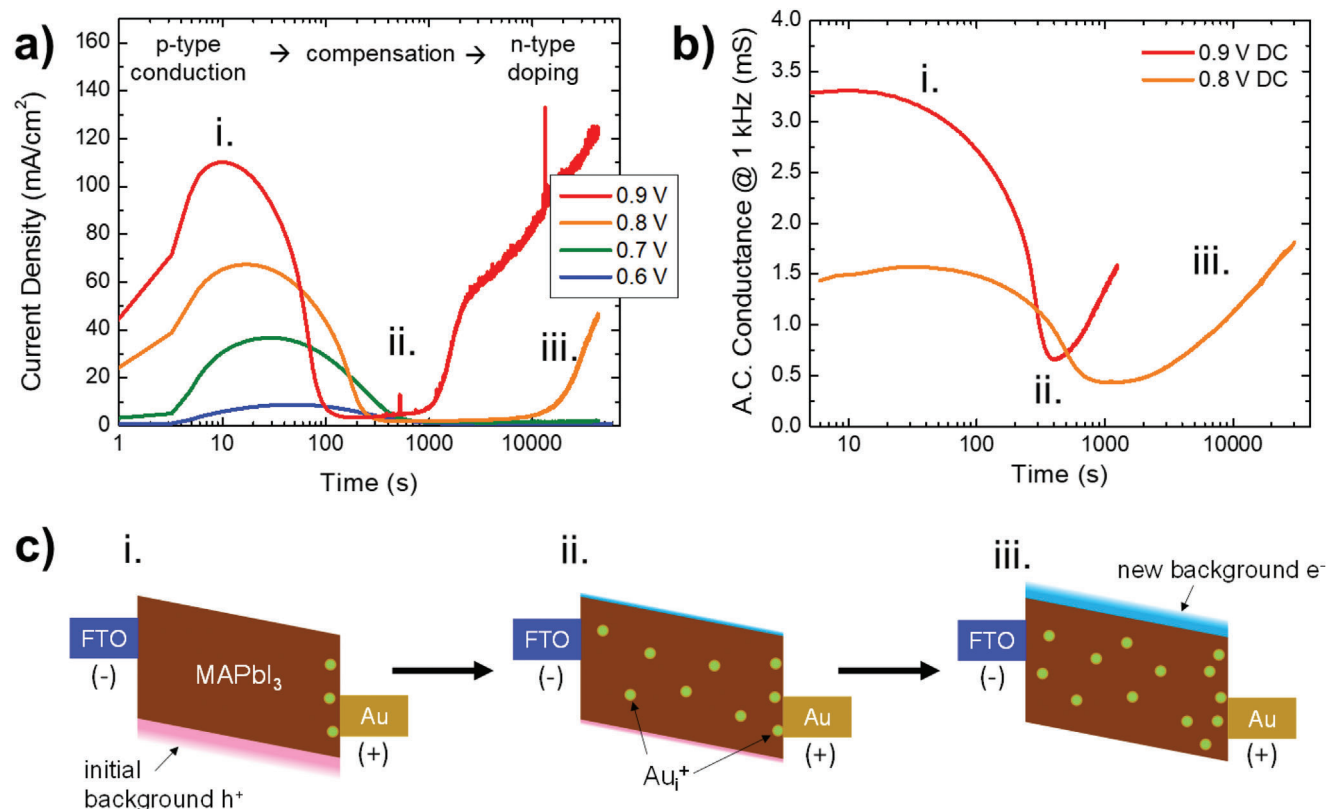
Figure 2. a) Current density–time (J–t, with logarithmic time scale) transients of solid-state FTO/MAPbI$_3$/Au devices biased at the indicated voltages, showing the proposed progression of p-type conduction, doping compensation, and n-type doping by electrochemical Au$_i^+$ formation. b) A.C. conductance measured at 1 kHz while the devices were held at the indicated DC voltages tracks with J–t transients. c) Qualitative device energy diagrams depicting the increasing Au$_i^+$ concentration and induced doping states at times i–iii indicated in (a) and (b).

2.2. FTO/MAPbI$_3$/Au Device Characterization

To isolate the formation and effect of the Au$_i^+$ defect, we fabricated and characterized model devices with an architecture of fluorine-doped tin oxide (FTO, ground/cathode/counter electrode)/MAPbI$_3$ ($\approx$500 nm thick)/Au (anode, 50–100 nm thick). This approach is intentional to ensure Au cations incorporate into the interstitial site as the dominant defect. Adding Au halide salts directly to the precursor solution would result in some Au incorporating on the B-site and may additionally induce higher concentrations of native defects that compensate doping. Presumably, our pre-formed perovskite has few A- and B-site vacancies and an abundance of vacant interstitial sites, so Au$_i^+$ should be the most likely species formed despite many defects being thermodynamically feasible.

In long-term potentiostatic measurements, we experimentally observe behavior consistent with compensation, n-doping, and re-equilibration (note that Au migration in this and other perovskite devices at these voltages is firmly established,[43–47] specifically with time-of-flight secondary-ion mass spectroscopy and energy-dispersive X-ray spectroscopy measurements for the present device architecture[43]). **Figure 2**a shows the J–t results of biasing individual pixels all from the same substrate, where each voltage condition is a fresh pixel, at the indicated voltages. The J–t transients are non-monotonic, and the evolution over time can be explained by the proposed Au$_i^+$ chemistry based on the

formation enthalpy trend in Figure 1b and assuming the perovskite bulk is initially p-type.[31,48] All pixels display a rapid initial increase in J in the first 10 s, which we attribute to near-interface-limited ion motion reducing hole injection barriers; an ionic process on this time scale is supported by electrochemical impedance spectroscopy (EIS) characterization (Figure S1 and Table S1, Supporting Information). The current then plateaus and is mainly supported by hole conduction. An applied bias of $V_{app} \approx 0.6$–0.7 V surmounts the formation energy and kinetic overpotentials to drive Au$_i^+$ into the perovskite bulk, where its compensation of holes causes a significant drop in J at intermediate time scales. At larger voltages, J increases again at long times as the sample becomes doped n-type. Last, the induced conductivity reverses over time after the bias is removed (Figure S2, Supporting Information), consistent with expectations for an electrolytic reaction and enthalpy of Au$_i^+$ formation >0 eV in n-type MAPbI$_3$ (Figure 1b). Notably, these dynamic doping phenomena are all induced at the indicated biases, suggesting the sum of the Gibbs free energy change and kinetic overpotentials to induce Au$_i^+$ formation are <0.6–0.8 eV, consistent with the magnitude of our computed formation enthalpy. We note that voltages >1 V cause heavy Au redistribution, to the point of forming Au^0 nanoparticles, which lie beyond the doping regime and are irrelevant for this work. We further note that negative bias merely reverses the reaction at the interface.

ADVANCED
SCIENCE NEWS
www.advancedsciencenews.com

ADVANCED
MATERIALS
www.advmat.de
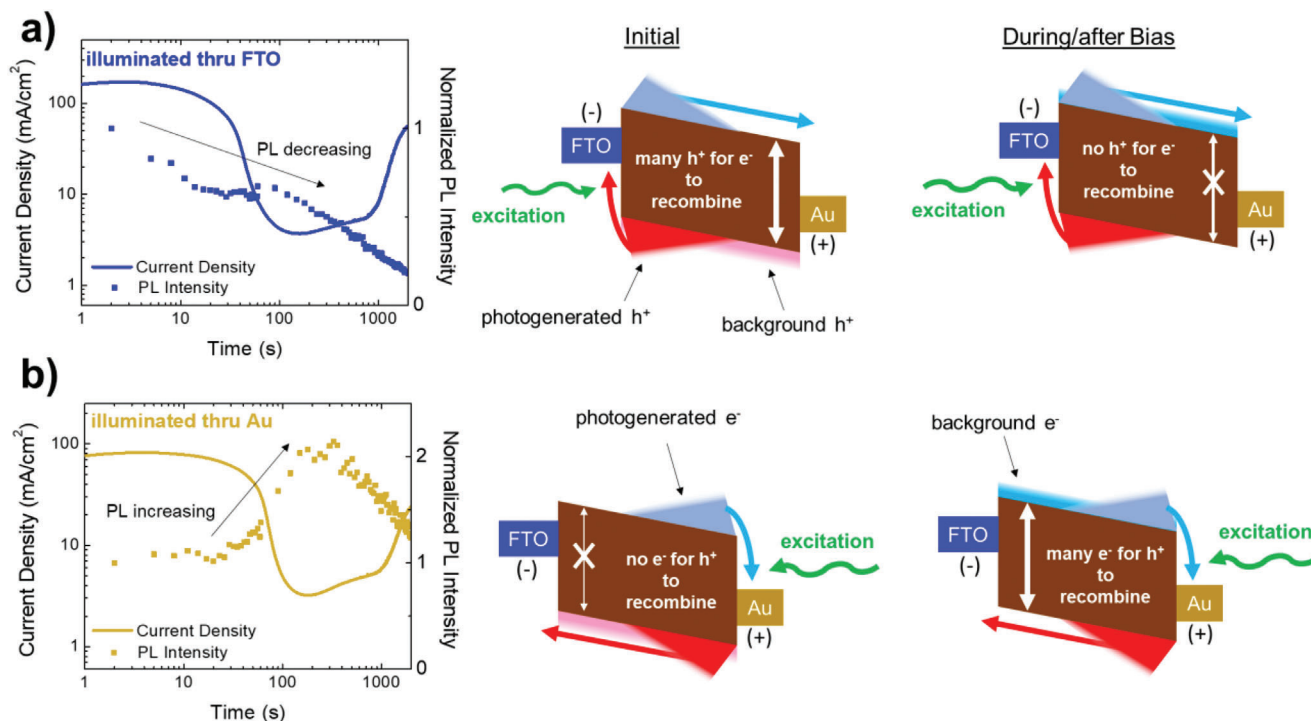
Figure 3. a,b) Current density versus time (J–t) at 0.9 V and in situ photoluminescence (PL) intensity of FTO/MAPbI$_3$/Au devices, where 532 nm PL excitation was applied through the FTO (a) or through the Au contact (b). Accompanying device energy diagrams (right) qualitatively illustrate the generation profiles of photocarriers and the direction the excess photogenerated carriers must travel through the device given the bias polarity. The white arrows indicate the probability of radiative recombination depends on the background carrier concentration that evolves from p-type to n-type over the length of the measurement.

To support p-type conduction in region i (Figure 2a), we confirmed that it arises from electronic conduction since Au$_i^+$ defects modulate carrier concentration, but do not contribute directly to J via an ionic current. This was concluded by monitoring the A.C. conductance ($1/|Z|$) over time at the indicated D.C. biases shown in Figure 2b. The A.C. conductance mirrors the J–t transient features in Figure 2a, suggesting the D.C. and A.C. response arise from the same charged species. Impedance spectroscopy and equivalent circuit analysis of a device before and after 0.9 V bias for 20–40 min additionally reveal a >10x increase in electronic conductivity, and there are no signatures of a large increase in ionic processes at low frequencies (Figure S1 and Table S1, Supporting Information). Moreover, the total charge passed through the device (obtained by integrating current density for the 0.7 V trace in Figure 2a between 1 and 600 s) would correspond to consumption of several micrometers thickness of Au metal, incompatible with the fact that only 50–100 nm were deposited for the electrodes. Thus, ionic current carried by Au$_i^+$ migration must be a negligible component of the current density in Figure 2a. In aggregate, these observations confirm that the non-monotonic J–t arises from changes in the electronic carrier concentrations to balance charge of Au$_i^+$ injected into the perovskite bulk. The change in background carrier concentration with increasing Au$_i^+$ over time is illustrated by the qualitative energy diagrams in Figure 2c.

In situ PL of FTO/MAPbI$_3$/Au devices provides additional device level support that the Au$_i^+$ is an n-dopant and that optoelectronic impacts can be observed. **Figure 3** shows the normalized

PL intensity of a device excited by 532 nm illumination through the FTO electrode (Figure 3a) and another through the Au contact (Figure 3b) during voltage bias. When illuminated through the FTO, the PL intensity decreases over time, whereas the PL intensity initially increases when excited through the Au (PL is stable for both conditions when no bias is applied, Figure S3, Supporting Information). This behavior can be explained by classic semiconductor device physics, noting that 532 nm excitation will asymmetrically generate photocarriers concentrated near the illuminated contact, as qualitatively illustrated in the device energy diagrams. These photocarriers must travel opposite directions through the device under voltage bias, as indicated by the arrows. Specifically, illuminating through the FTO, holes will be rapidly collected by the FTO cathode while the electrons will need to traverse the perovskite thickness to be collected at the Au anode. Along the way, the electrons may recombine with the background hole density if the perovskite is initially p-type. However, as the Au$_i^+$ doping compensates the holes and eventually induces n-type doping, the photogenerated electrons will see a diminishing background hole population with which to recombine during transit, in which case PL intensity should decrease over time as observed. This is corroborated by repeating the measurement with 640 nm excitation generating carriers more homogeneously across the device, in which case PL is less affected by the background concentration (Figure S4, Supporting Information). Conversely, when excited through the Au, the opposite is true; electrons are generated nearby the Au anode for collection, photogenerated holes must traverse the thickness of the device, and

an increasing concentration of background n-doping under bias would increase the probability of excess holes radiatively recombining to increase PL intensity as observed in Figure 3b. At times >300 s, the formation of Au^0 colloids[43] likely causes the PL intensity to decrease for all excitation conditions.

It remains possible that mobile ions have some influence on our experiment via trap filling, passivation, or other effects on radiative/non-radiative recombination. However, the $Au_i^{+/0}$ charge transition level, calculated to lie near or within the conduction band in Figure 1b, predicts that Au_i^+ should not introduce a non-radiative recombination pathway. Indeed, if it did, we would expect PL excited through the Au contact in Figure 3b to be quenched soon after voltage is applied, yet the opposite is observed. Second order effects including defects and trap filling are beyond the scope here, as our analysis of the in situ PL is, to first order, adequately explained by considering bias polarity of the device, photocarrier generation profiles, and background doping evolution induced by the Au_i^+ electrochemistry.

2.3. Generality to Other Systems

Figure 4a,b shows J–t measurements of FTO/$Cs_{0.05}FA_{0.79}MA_{0.16}$-$Pb(I_{0.83}Br_{0.17})_3$/Au and FTO/$Cs_{0.15}FA_{0.85}PbI_3$:Cl/Au, respectively (FA = formamidinium). The transients follow the same general behavior as for $MAPbI_3$ (see Figure S5, Supporting Information, for recovery behavior), demonstrating the above-deduced Au_i^+ electrochemistry is qualitatively unaffected by differences in perovskite A-site cation composition, morphology, and defect concentrations. This is reasonable, given that the reaction is between Au^0 and an empty interstitial site which are both abundant at a perovskite/Au interface. Both alloys in Figure 4 display somewhat less pronounced J–t features compared to $MAPbI_3$. We attribute this behavior to sample inhomogeneity exacerbated by mixed cation and anion compositions; abundant compositional and electronic inhomogeneity lead to p-type and n-type regions at spatially separate regions evolving simultaneously, but independently, within the device. Regardless, the general p-type to intrinsic and intrinsic to n-type evolution is observed irrespective of perovskite composition.

It is interesting to note that, while it still displays the doping transients, the $Cs_{0.15}FA_{0.85}PbI_3$ composition also differs from the MA-containing compositions in that Au migration is often not as easily detected (Figures S6 and S7, Supporting Information). A suppressed reaction with Au has also been claimed for $FAPbI_3$ crystals.[49] This is consistent with recently reported effects of the A-site cation on defect stability,[50] as well as on migration properties.[51] Specifically, in $MAPbI_3$ and related compositions, we suspect that Au cations are stable in the interstitial position compared to the octahedral centers (B-site) in phases like $MA_2Au_2Br_6$[45] or $MA_2Au_2I_6$.[52] Instead, CsFA systems may prefer Au cations to occupy sites resembling $Cs_2Au_2I_6$,[53,54] or $FA_2Au_2I_6$ (hypothetical) where the cations in B-sites are much less mobile,[55] and a surface restructuring or phase modification may remove interstitial sites available to react; the net result cuts off Au migration pathways. Future studies on this class of doping mechanisms will require in depth computations on competing reactions and phases.
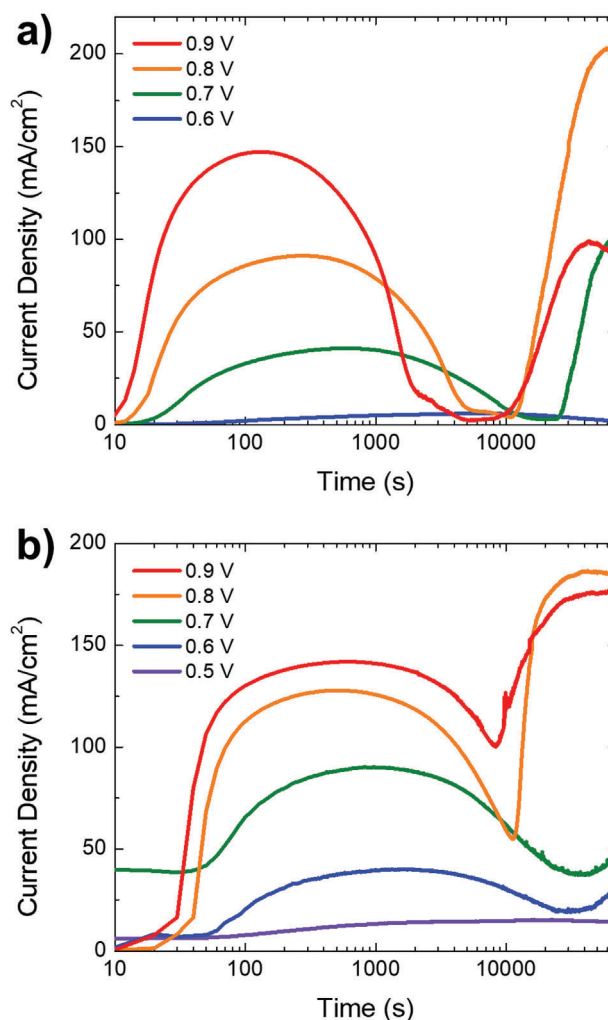
Figure 4. a,b) Current density–time (J–t) transients of FTO/$Cs_{0.05}FA_{0.79}$-$MA_{0.16}Pb(I_{0.83}Br_{0.17})_3$/Au (a) and FTO/$Cs_{0.15}FA_{0.85}PbI_3$:Cl/Au (b) devices, biased at the indicated voltages showing similar characteristics as FTO/$MAPbI_3$/Au (cf. Figure 2a).

Finally, many extrinsic metal cations are capable of occupying interstitial sites,[39,40] so we examined Ag_i^+ by characterizing a FTO/$MAPbI_3$/Ag device (Figure S8, Supporting Information) as well as a FTO/$Cs_{0.05}FA_{0.79}MA_{0.16}Pb(I_{0.83}Br_{0.17})_3$/Ag device shown in **Figure 5**. The J–t transients (Figure 5a) and recovery behavior (Figure S9, Supporting Information) are qualitatively similar to devices with an Au anode. Small differences between the Ag- and Au-device J–t transients are consistent with predicted properties of Au_i^+ versus Ag_i^+, strengthening the relationship between theory and experiment supporting this class of defects. Specifically, the lower voltage thresholds (≈0.08 V versus 0.8 V) are explained by Ag_i^+ formation enthalpy curve shifted to lower values relative to Au_i^+.[39,56] Additionally, faster time scales for Ag-doping are predicted by Ag_i^+ migration energies computed to be ≈0.15 eV lower than for Au_i^+, suggesting Ag_i^+ migration rates may be 100× faster than Au_i^+.[39,40] A detailed discussion can be found in Note I in the SI (Supporting Information). Overall, the measurements and interpretation of Ag and Ag_i^+ corroborate our

**ADVANCED
SCIENCE NEWS**

www.advancedsciencenews.com

**ADVANCED
MATERIALS**

www.advmat.de
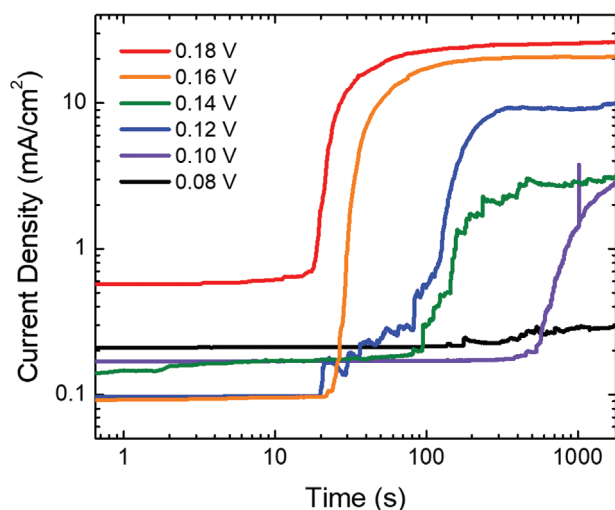
Figure 5. Current density–time (J–t) transients of a FTO/$Cs_{0.05}FA_{0.79}$-$MA_{0.16}Pb(I_{0.83}Br_{0.17})_3$/Ag device.

analysis of Au_i^+ and increase our confidence in the formation and observable impacts of doping by noble metal cation interstitials in halide perovskite devices generally.

2.4. Implications for Halide Perovskite Technologies

Our study focuses on Au_i^+ and Ag_i^+ defects because noble metal electrodes are stable enough to study by applying small voltages, yet they should not be assumed to be unreactive. Indeed, noble metal migration in perovskite photovoltaics is common and comes at the risk of degradation.[44,46,47] Solutions may lie in improved ionic barrier layers or exploitation of phases like $Cs_{0.15}FA_{0.85}PbI_3$ that may intrinsically suppress interstitial migration, as revealed for Au_i^+ by this work (see Figures S6 and S7, Supporting Information). Whether the interstitial-induced doping effect is beneficial or detrimental depends strongly on the type and details of any specific device.[57] For example, doping may be beneficial in light-emitting diodes. But a device with an Au anode may feature transients to current density or electroluminescence, as well as hysteretic behavior, which may be viewed as a specific instability intrinsic to this type of interface. One type of device which may benefit from the above-discussed phenomena is the neuromorphic memristor, in which uniformly distributed interstitial doping by electrochemical reactions with metal electrodes represents a new mechanism to switch polarity in halide perovskite photovoltaic devices[4–6] and switch between resistance states in neuromorphic devices.[49,58–62]

Irrespective of the end application, it should now be abundantly clear that use of direct Au electrodes for quantification of doping levels by techniques including Hall effect, space-charge-limited current (SCLC), and capacitance–voltage measurements should be avoided, as the application of even a small voltage bias dynamically changes the doping state of the perovskite material leading to unreliable or erroneous results. Determining these doping changes ex situ by surface techniques like Kelvin probe or electron photoemission necessitate deconstruction of the device and formation of new surfaces, which introduce significant

uncertainty due to induced surface reactions.[6,63] The doping we describe here is a device level phenomenon—it cannot occur without the perovskite sandwiched between two electrodes under bias—and in situ characterization that preserve this state must be employed, examples of which we have presented.

The above concepts can be applied more broadly to better predict the behavior of other extrinsic interstitial defects, including plausible redox reactions with native perovskite defects such as I_i^+. The range corresponding to reported I_i charge transition levels lies around midgap, as indicated in Figure 1b;[34,36] it may therefore be favorable for Au^0 to react with any holes or positive I_i^+ defects initially present in the material via reactions **1** and **2**. Reaction **2** can be equivalently viewed as some I_i^+ converting to I_i^- as the Au_i^+ n-doping moves the Fermi energy upward toward midgap. A spontaneous reaction between I_i^+ and Au^0 may further explain the slight Au migration observed in control and sub-threshold biased devices here (Figure S6, Supporting Information) as well as in our previous study, where it was attributed to defect reactions more generally.[43] We envision opportunities to exploit these ionic–electronic processes to impose control over the oxidation state of defects like I_i or defect-pair complexes[56] that could be engineered to improve optoelectronic properties beyond doping.

3. Conclusion

We have reported electrochemically induced migration of Au and Ag in halide perovskite devices and observed effects on electronic conduction and optoelectronic behavior consistent with computational predictions for Au^+ and Ag^+ interstitial defects. Our analysis and approach strengthen the bridge between experiment and theory for halide perovskite interstitial defects to help push beyond a state of qualitative relationships and facilitate future semiquantitative or quantitative studies. This represents a significant advance in perovskite technological development and progress toward reconciling "unconventional" characteristics of halide perovskites, such as mobile ions and defect redox chemistry, with textbook semiconductor physics. Further work on extrinsic interstitials will solidify an accurate understanding of their optoelectronic consequences and facilitate strategies to leverage this type of dynamic doping in halide perovskites for traditional semiconductor applications as well as for novel neuromorphic devices.

4. Experimental Section

Experimental details are provided in Supporting Information.

Supporting Information

Supporting Information is available from the Wiley Online Library or from the author.

Conflict of Interest

The authors declare no conflict of interest.

Data Availability Statement

The data that support the findings of this study are available from the corresponding author upon reasonable request.

Keywords

electrochemical doping, halide perovskite, interstitial defects

[1] E. Amerling, H. Lu, B. W. Larson, A. E. Maughan, A. Phillips, E. Lafalce, L. Whittaker-Brooks, J. J. Berry, M. C. Beard, Z. V. Vardeny, J. L. Blackburn, *ACS Energy Lett.* **2021**, *6*, 1104.

[2] J. Euvrard, Y. Yan, D. B. Mitzi, *Nat. Rev. Mater.* **2021**, *6*, 531.

[3] G. Richardson, S. E. J. O'Kane, R. G. Niemann, T. A. Peltola, J. M. Foster, P. J. Cameron, A. B. Walker, *Energy Environ. Sci.* **2016**, *9*, 1476.

[4] Y. Zhao, C. Liang, H. Zhang, D. Li, D. Tian, G. Li, X. Jing, W. Zhang, W. Xiao, Q. Liu, F. Zhang, Z. He, *Energy Environ. Sci.* **2015**, *8*, 1256.

[5] Z. Xiao, Y. Yuan, Y. Shao, Q. Wang, Q. Dong, C. Bi, P. Sharma, A. Gruverman, J. Huang, *Nat. Mater.* **2015**, *14*, 193.

[6] R. A. Kerner, P. Schulz, J. A. Christians, S. P. Dunfield, B. Dou, L. Zhao, G. Teeter, J. J. Berry, B. P. Rand, *APL Mater.* **2019**, *7*, 041103.

[7] S. Zhou, Y. Ma, G. Zhou, X. Xu, M. Qin, Y. Li, Y.-J. Hsu, H. Hu, G. Li, N. Zhao, J. Xu, X. Lu, *ACS Energy Lett.* **2019**, *4*, 534.

[8] S. Zhou, G. Zhou, Y. Li, X. Xu, Y.-J. Hsu, J. Xu, N. Zhao, X. Lu, *ACS Energy Lett.* **2020**, *5*, 2614.

[9] R. Begum, M. R. Parida, A. L. Abdelhady, B. Murali, N. M. Alyami, G. H. Ahmed, M. N. Hedhili, O. M. Bakr, O. F. Mohammed, *J. Am. Chem. Soc.* **2017**, *139*, 731.

[10] N. Phung, R. Félix, D. Meggiolaro, A. Al-Ashouri, G. Sousa e Silva, C. Hartmann, J. Hidalgo, H. Köbler, E. Mosconi, B. Lai, R. Gunder, M. Li, K.-L. Wang, Z.-K. Wang, K. Nie, E. Handick, R. G. Wilks, J. A. Marquez, B. Rech, T. Unold, J.-P. Correa-Baena, S. Albrecht, F. De Angelis, M. Bär, A. Abate, *J. Am. Chem. Soc.* **2020**, *142*, 2364.

[11] A. L. Abdelhady, M. I. Saidaminov, B. Murali, V. Adinolfi, O. Voznyy, K. Katsiev, E. Alarousu, R. Comin, I. Dursun, L. Sinatra, E. H. Sargent, O. F. Mohammed, O. M. Bakr, *J. Phys. Chem. Lett.* **2016**, *7*, 295.

[12] P. Sarkar, A. Srivastava, S. K. Tripathy, K. L. Baishnab, T. R. Lenka, P. S. Menon, F. Lin, A. G. Aberle, *J. Appl. Phys.* **2020**, *127*, 125110.

[13] Z. Yang, M. Wei, O. Voznyy, P. Todorovic, M. Liu, R. Quintero-Bermudez, P. Chen, J. Z. Fan, A. H. Proppe, L. N. Quan, G. Walters, H. Tan, J.-W. Chang, U.-S. Jeng, S. O. Kelley, E. H. Sargent, *J. Am. Chem. Soc.* **2019**, *141*, 8296.

[14] Y. Zhou, J. Chen, O. M. Bakr, H.-T. Sun, *Chem. Mater.* **2018**, *30*, 6589.

[15] B. Luo, F. Li, K. Xu, Y. Guo, Y. Liu, Z. Xia, J. Z. Zhang, *J. Mater. Chem. C* **2019**, *7*, 2781.

[16] A. Zohar, I. Levine, S. Gupta, O. Davidson, D. Azulay, O. Millo, I. Balberg, G. Hodes, D. Cahen, *ACS Energy Lett.* **2017**, *2*, 2408.

[17] A. Senocrate, I. Moudrakovski, G. Y. Kim, T.-Y. Yang, G. Gregori, M. Grätzel, J. Maier, *Angew. Chem., Int. Ed.* **2017**, *56*, 7755.

[18] A. R. Kirmani, A. E. Mansour, C. Yang, R. Munir, A. M. El-Zohry, O. F. Mohammed, A. Amassian, *PLoS One* **2020**, *15*, e0230540.

[19] F. Zhang, H. L. Smith, A. Kahn, *Appl. Phys. Rev.* **2021**, *8*, 041301.

[20] E. A. Gaulding, J. Hao, H. S. Kang, E. M. Miller, S. N. Habisreutinger, Q. Zhao, A. Hazarika, P. C. Sercel, J. M. Luther, J. L. Blackburn, *Adv. Mater.* **2019**, *31*, 1902250.

[21] N. K. Noel, S. N. Habisreutinger, A. Pellaroque, F. Pulvirenti, B. Wenger, F. Zhang, Y.-H. Lin, O. G. Reid, J. Leisen, Y. Zhang, S. Barlow, S. R. Marder, A. Kahn, H. J. Snaith, C. B. Arnold, B. P. Rand, *Energy Environ. Sci.* **2019**, *12*, 3063.

[22] E. E. Perry, J. G. Labram, N. R. Venkatesan, H. Nakayama, M. L. Chabinyc, *Adv. Electron. Mater.* **2018**, *4*, 1800087.

[23] D. Shin, F. Zu, A. V. Cohen, Y. Yi, L. Kronik, N. Koch, *Adv. Mater.* **2021**, *33*, 2100211.

[24] J. Euvrard, O. Gunawan, X. Zhong, S. P. Harvey, A. Kahn, D. B. Mitzi, *Mater. Adv.* **2021**, *2*, 2956.

[25] S. Heo, K. Roh, F. Zhang, S. E. Tignor, A. B. Bocarsly, A. Kahn, B. P. Rand, *ACS Energy Lett.* **2022**, *7*, 211.

[26] Q. Jiang, X. Zeng, N. Wang, Z. Xiao, Z. Guo, J. Lu, *ACS Energy Lett.* **2018**, *3*, 264.

[27] J. T. Mulder, I. du Fossé, M. Alimoradi Jazi, L. Manna, A. J. Houtepen, *ACS Energy Lett.* **2021**, *6*, 2519.

[28] Q. Jiang, M. Chen, J. Li, M. Wang, X. Zeng, T. Besara, J. Lu, Y. Xin, X. Shan, B. Pan, C. Wang, S. Lin, T. Siegrist, Q. Xiao, Z. Yu, *ACS Nano* **2017**, *11*, 1073.

[29] S. G. Motti, D. Meggiolaro, A. J. Barker, E. Mosconi, C. A. R. Perini, J. M. Ball, M. Gandini, M. Kim, F. De Angelis, A. Petrozza, *Nat. Photon.* **2019**, *13*, 532.

[30] K. X. Steirer, P. Schulz, G. Teeter, V. Stevanovic, M. Yang, K. Zhu, J. J. Berry, *ACS Energy Lett.* **2016**, *1*, 360.

[31] F. Zu, C. M. Wolff, M. Ralaiarisoa, P. Amsalem, D. Neher, N. Koch, *ACS Appl. Mater. Interfaces* **2019**, *11*, 21578.

[32] P. Schulz, L. L. Whittaker-Brooks, B. A. MacLeod, D. C. Olson, Y.-L. Loo, A. Kahn, *Adv. Mater. Interfaces* **2015**, *2*, 1400532.

[33] M.-H. Du, *J. Phys. Chem. Lett.* **2015**, *6*, 1461.

[34] X. Zhang, M. E. Turiansky, J.-X. Shen, C. G. Van de Walle, *Phys. Rev. B* **2020**, *101*, 140101.

[35] M. W. Swift, J. L. Lyons, *J. Mater. Chem. A* **2021**, *9*, 7491.

[36] D. Meggiolaro, S. G. Motti, E. Mosconi, A. J. Barker, J. Ball, C. A. R. Perini, F. Deschler, A. Petrozza, F. D. Angelis, *Energy Environ. Sci.* **2018**, *11*, 702.

[37] S. D. Stranks, V. M. Burlakov, T. Leijtens, J. M. Ball, A. Goriely, H. J. Snaith, *Phys. Rev. Appl.* **2014**, *2*, 034007.

**ADVANCED
SCIENCE NEWS**

www.advancedsciencenews.com

**ADVANCED
MATERIALS**

www.advmat.de

[38] D. Yang, W. Ming, H. Shi, L. Zhang, M.-H. Du, *Chem. Mater.* **2016**, *28*, 4349.

[39] W. Ming, D. Yang, T. Li, L. Zhang, M.-H. Du, *Adv. Sci.* **2018**, *5*, 1700662.

[40] Y. Liang, X. Cui, F. Li, C. Stampfl, S. P. Ringer, R. Zheng, *npj Comput. Mater.* **2021**, *7*, 63.

[41] A. V. Cohen, D. A. Egger, A. M. Rappe, L. Kronik, *J. Phys. Chem. Lett.* **2019**, *10*, 4490.

[42] C. Freysoldt, B. Grabowski, T. Hickel, J. Neugebauer, G. Kresse, A. Janotti, C. G. Van de Walle, *Rev. Mod. Phys.* **2014**, *86*, 253.

[43] R. A. Kerner, L. Zhao, S. P. Harvey, J. J. Berry, J. Schwartz, B. P. Rand, *ACS Energy Lett.* **2020**, *5*, 3352.

[44] K. Domanski, J.-P. Correa-Baena, N. Mine, M. K. Nazeeruddin, A. Abate, M. Saliba, W. Tress, A. Hagfeldt, M. Grätzel, *ACS Nano* **2016**, *10*, 6306.

[45] J. Wang, S. P. Senanayak, J. Liu, Y. Hu, Y. Shi, Z. Li, C. Zhang, B. Yang, L. Jiang, D. Di, A. V. Ievlev, O. S. Ovchinnikova, T. Ding, H. Deng, L. Tang, Y. Guo, J. Wang, K. Xiao, D. Venkateshvaran, L. Jiang, D. Zhu, *Adv. Mater.* **2019**, *31*, 1902618.

[46] S. Cacovich, L. Ciná, F. Matteocci, G. Divitini, P. A. Midgley, A. D. Carlo, C. Ducati, *Nanoscale* **2017**, *9*, 4700.

[47] Y. Jiang, S.-C. Yang, Q. Jeangros, S. Pisoni, T. Moser, S. Buecheler, A. N. Tiwari, F. Fu, *Joule* **2020**, *4*, 1087.

[48] F. Zu, D. Shin, N. Koch, *Mater. Horiz.* **2022**, *9*, 17.

[49] C. Ma, B. Kim, D.-H. Kang, S.-W. Kim, N.-G. Park, *ACS Energy Lett.* **2021**, *6*, 2817.

[50] D. R. Ceratti, A. V. Cohen, R. Tenne, Y. Rakita, L. Snarski, N. P. Jasti, L. Cremonesi, R. Cohen, M. Weitman, I. Rosenhek-Goldian, I. Kaplan-Ashiri, T. Bendikov, V. Kalchenko, M. Elbaum, M. a. C. Potenza, L. Kronik, G. Hodes, D. Cahen, *Mater. Horiz.* **2021**, *8*, 1570.

[51] A. Oranskaia, J. Yin, O. M. Bakr, J.-L. Brédas, O. F. Mohammed, *J. Phys. Chem. Lett.* **2018**, *9*, 5474.

[52] N. N. Shlenskaya, N. A. Belich, M. Grätzel, E. A. Goodilin, A. B. Tarasov, *J. Mater. Chem. A* **2018**, *6*, 1780.

[53] H. Kitagawa, N. Kojima, N. Matsushita, T. Ban, I. Tsujikawa, *J. Chem. Soc., Dalton Trans.* **1991**, *11*, 3115.

[54] H. Kitagawa, N. Kojima, T. Nakajima, *J. Chem. Soc., Dalton Trans.* **1991**, *11*, 3121.

[55] C. P. Clark, J. E. Mann, J. S. Bangsund, W.-J. Hsu, E. S. Aydil, R. J. Holmes, *ACS Energy Lett.* **2020**, *5*, 3443.

[56] M. W. Swift, J. L. Lyons, *J. Phys. Chem. C* **2022**, *126*, 12294.

[57] A. W. Stewart, A. Julien, D. Regaldo, P. Schulz, B. Marí Soucase, D. R. Ceratti, P. López-Varo, *Mater. Today Chem.* **2023**, *29*, 101380.

[58] Y. Sun, M. Tai, C. Song, Z. Wang, J. Yin, F. Li, H. Wu, F. Zeng, H. Lin, F. Pan, *J. Phys. Chem. C* **2018**, *122*, 6431.

[59] G. T. S. How, N. A. Talik, B. K. Yap, H. Nakajima, S. Tunmee, B. T. Goh, *Appl. Surf. Sci.* **2019**, *473*, 194.

[60] J. S. Han, Q. V. Le, J. Choi, H. Kim, S. G. Kim, K. Hong, C. W. Moon, T. L. Kim, S. Y. Kim, H. W. Jang, *ACS Appl. Mater. Interfaces* **2019**, *11*, 8155.

[61] X. Zhu, J. Lee, W. D. Lu, *Adv. Mater.* **2017**, *29*, 1700527.

[62] Y. Wang, Z. Lv, L. Zhou, X. Chen, J. Chen, Y. Zhou, V. a. L. Roy, S.-T. Han, *J. Mater. Chem. C* **2018**, *6*, 1600.

[63] F. Zhang, F. Ullrich, S. Silver, R. A. Kerner, B. P. Rand, A. Kahn, *J. Phys. Chem. Lett.* **2019**, *10*, 890.

2302206 (8 of 8)